Origin of cluster and void structure in melt-quenched Fe-Co-B metallic glasses determined by positron annihilation at low temperatures

K. Krištiaková and P. Švec
Institute of Physics, Slovak Academy of Sciences, Dúbravská Cesta 9, 84228 Bratislava, Slovakia
(Received 1 December 1999; revised manuscript received 23 February 2000; published 14 June 2001)

The microstructure, type of short-range ordering, and occurrence of free volume in $Fe_{64}Co_{21}B_{15}$ metallic glass ribbons quenched from the melt have been analyzed by positron annihilation lifetime spectroscopy (PALS) at 300 K and at 20 K. The combined results from PALS and electrical resistivity measurements performed at both temperatures point to different types of metal-metalloid neighborhood with corresponding specific types and populations of capture sites. A special method for analysis of the annihilation rate probability density function $f(\lambda)$ was used to separate and identify positron capture sites of different size and origin. An analysis of the results has permitted the assignment of these different sites to disordered groups of metallic atoms and to metal-metalloid clusters that were probably directly frozen in from the melt.

DOI: 10.1103/PhysRevB.64.014204 PACS number(s): 78.70.Bj, 61.43.Dq, 61.46.+w

I. INTRODUCTION

The metastable and disordered state of metal-metalloid amorphous alloys still poses open questions about the existence of ordering on the atomic scale within such alloys, especially about the existence of clusters consisting of several metal and metalloid atoms, the type, number, structure, genesis, and stability of such clusters, and the structure of the matrix surrounding such clusters. For a long time it was supposed that amorphous metallic alloys can be modeled or physically prepared from atoms of individual components put into a disordered state by simple melting and sufficiently rapid quenching to prevent establishment of equilibrium (crystalline) atomic structure. The simulated atomic structure obtained via such simple model constructions,[1,2] however, does not behave in a similar fashion to realistic systems, which are known to exhibit a higher degree of short-range order (SRO); see, e.g., Ref. 3. In reality the preparation of fully amorphous metallic glasses is usually a two-stage process[4] with the system passing through the melting temperature to the liquid state twice, inducing effects that ought to be of primary importance for the formation of a glassy structure. In spite of progress in theoretical approaches, computing facilities, and advances in numerical methods, there exists no first-principles model for amorphous metallic systems, due to the inapplicability of a periodic potential to disordered structures; any low-energy structural unit or cluster has to be postulated *a priori*. Further complications for modeling are caused by the presence of $3d$ atoms, by electron localization, and by combinations of metals and metalloids in real systems.

The possibilities for investigation of the cluster structure depend on the effect that the changes of the cluster structure have on the overall atomic structure, properties, and stability of the amorphous matter. An ideal case is when the amorphous matter is composed of phases with different cluster types and selective heat treatment is capable of bringing about changes in one type of cluster only, as, for example, in the case of samples where undercooled liquid and amorphous solid coexist, such as Ni-Zr-Al based alloys.[5] Another, more difficult, possibility in the case when a single type of cluster structure is expected (e.g., in metal-metalloid amorphous systems), is either to induce changes in the cluster structure in the course of its formation (e.g., while still in the molten state[4]) or to investigate the changes in the amorphous matter and interpret the stability and evolution of the cluster structure upon transition from amorphous to crystalline states.

Positron annihilation lifetime spectroscopy (PALS) is capable of providing direct information about the process of clustering in metallic glasses. Positrons in bulk material image vacant spaces where atoms are missing (in a crystalline structure) or where the density of the atoms is reduced (as in subvacancy-sized small free volumes, excess free volume, open spaces or voids in disordered condensed matter).[4,5] In the present work we attempted to investigate the positron capture sites and the corresponding SRO surrounding these sites in selected Fe-Co-B samples and to follow the stability of these sites against structural transformations.

II. EXPERIMENT

A. Sample selection, preparation, and annealing

The amorphous metallic alloy $Fe_{64}Co_{21}B_{15}$ is a ternary alloy at the lower limit of glass forming ability in the Fe-Co-B system. This alloy represents the basic composition for the preparation of special nanocrystalline soft magnetic systems of the Fe-Co-B type with additions of Nb, Zr, or Hf exhibiting the highest known saturation magnetization.[6] It contains a low amount of boron, yet, in contrast to binary $Fe_{85}B_{15}$, crystallizes in two well-separated stages, which makes it convenient for investigation of the evolution of the cluster structure as crystallization proceeds. The crystallization mechanism of this amorphous alloy has been investigated previously in detail in Ref. 7. Low-temperature mechanical properties of Fe-Co-B metallic glasses, especially thermal expansion at low temperatures, and their connection with microstructure were discussed in Ref. 8. The influence of the melt history and casting conditions on the degree of clustering is well known from detailed studies utilizing PALS.[4] In that work the clustering process was correlated with the history of the master alloy in the molten state.

The master alloy and sample preparation conditions were the same as those commonly used for the preparation of

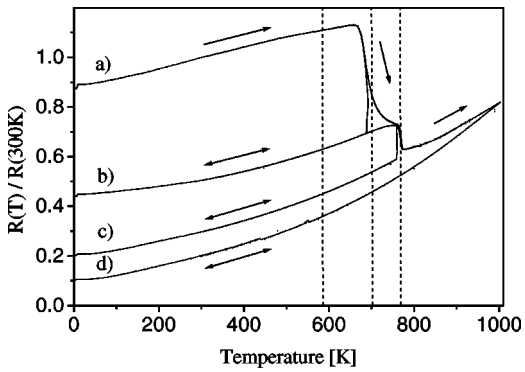

FIG. 1. Temperature dependence of electrical resistivity for four stages of thermal treatment: (a) as-quenched amorphous sample, (b) sample after first crystallization, (c) sample after second crystallization, and (d) sample heated to 1000 K. Dashed vertical lines indicate selected annealing temperatures.

Fe-Co-B metallic glasses by planar flow casting. This process involves the already mentioned two-stage preparation process. The master alloy was prepared from the elements with 99.9% purity in a vacuum induction furnace by heating the master alloy melt up to 1523 K. Amorphous ribbons 6 mm wide and 25.2 ± 0.1 μm thick were prepared from the polycrystalline master alloy at 1523 K by the planar flow casting method on a copper wheel rotating with the velocity of 30 ± 1 m s^{-1}. The chemical composition of both the master alloy and the amorphous ribbon was checked by inductionally coupled plasma spectroscopy to verify the desired nominal composition of the alloy to an accuracy of 0.1% of the elemental content and to confirm the absence of impurities, especially carbides and oxides, within the ribbon. X-ray analysis was performed using Cu$K\alpha$ radiation and the Bragg-Brentano measuring configuration. X-ray diffraction of the as-cast ribbon revealed no presence of as-quenched crystalline phases. The samples were confirmed to be fully amorphous in the as-cast state by detailed transmission electron microscopy (TEM) and selected-area electron diffraction (ED) performed at different places along the length and across the thickness of the ribbon. Samples for TEM and ED were thinned by ion-beam milling.

Electrical resistivity measurements were performed using a high-precision four-point probe method in a cryostat in the temperature range 4.2 to 320 K and from 300 to 1100 K in a high-vacuum furnace with pressure less than 10^{-4} Pa using 7 K/min heating rate. Measurements have been performed on as-quenched as well as annealed samples to estimate the temperature dependence of electrical resistivity of the as-quenched and thermally treated metallic glass in a wide temperature range. The results of the electrical resistivity measurements are shown in Fig. 1. From these measurements three annealing temperatures were selected to accentuate different neighborhoods of anticipated (FeCo)-B clusters. Measurements were performed on amorphous (as-quenched) samples, on samples relaxed in the vacuum furnace at 573 K for 3 h to anneal out stresses, on samples annealed at 693 K for 1 h, and on samples anealed at 767 K for 1 h. The choice of stress relief annealing parameters (573 K for 3 h) represents a compromise between the highest annealing temperature and time for relaxation to take place and yet to ensure no crystallization; no surface oxidation or surface crystallization were detected. The annealing at 693 K was selected to prepare samples just after the end of the first crystallization reaction in order to see the influence of the crystallization products from the first crystallization reaction together with the remaining amorphous metalloid-rich matrix on the cluster structure. The last group of samples annealed at 767 K, i.e., after the second crystallization reaction, provides a fully crystallized structure. After each annealing the samples were checked for the type of crystalline structure formed by x-ray spectroscopy and TEM. After the first crystallization stage about 50 vol % is transformed to bcc α-(Fe-Co) in the form of regular star-shaped crystals about 100 nm in size. During the second crystallization reaction $(FeCo)_3B$ borides are formed from the remaining amorphous matrix. Details about the types of phase formed, crystalline phase morphology, kinetics of crystallization, and nucleation rates are in Ref. 7.

B. Positron annihilation lifetime method and data processing

The positron annihilation lifetime spectra as well as the instrument resolution function were obtained in the same way detailed in previous work.[4,5] The first set of lifetime spectra was measured at room temperature, while the second set of spectra was measured at 20 K in a closed-cycle helium gas refrigerator with automatic temperature regulation. The sample-source assembly was completely enclosed in an evacuated copper holder placed at the end of the cold finger of the refrigerator.

A specimen for positron annihilation lifetime measurement consisted of two stacks of 12 layers of the sample material with the positron source sandwiched between them in order to ensure the annihilation of positrons within the volume of the samples.

Both sets of experimental positron lifetime spectra were analyzed by the Laplace inversion technique using the modified CONTIN (PALS-2) program[9] which deconvolutes the time spectra into the annihilation rate probability density function (PDF) $\alpha(\lambda)$ as a function of annihilation rate λ via constrained regularized least-squares solution of the Fredholm integral equation with the normalization condition $\int_0^\infty \alpha(\lambda) d\lambda = 1$. A deconvolution algorithm based on the principle of parsimony ensures the choice of the smoothest solution, i.e., the smallest number of lifetimes with respect to the number of degrees of freedom. For convenience, when λ ranges over a larger interval of values, the annihilation rate PDF as a function of the logarithm of λ is expressed as $f(\lambda) = \lambda \alpha(\lambda)$ and is also transformed to the annihilation lifetime representation, where $\tau = 1/\lambda$ is the annihilation lifetime. Conversion of the annihilation rate PDF to the annihilation lifetime PDF requires a transformation of the variable of integration, because the PDF is not invariant against the transformation of variables from λ to τ. The fraction of positrons annihilating with lifetimes between τ and $\tau + d\tau$ is $\lambda^2 \alpha(\lambda) d\tau$. Thus the corresponding annihilation lifetime

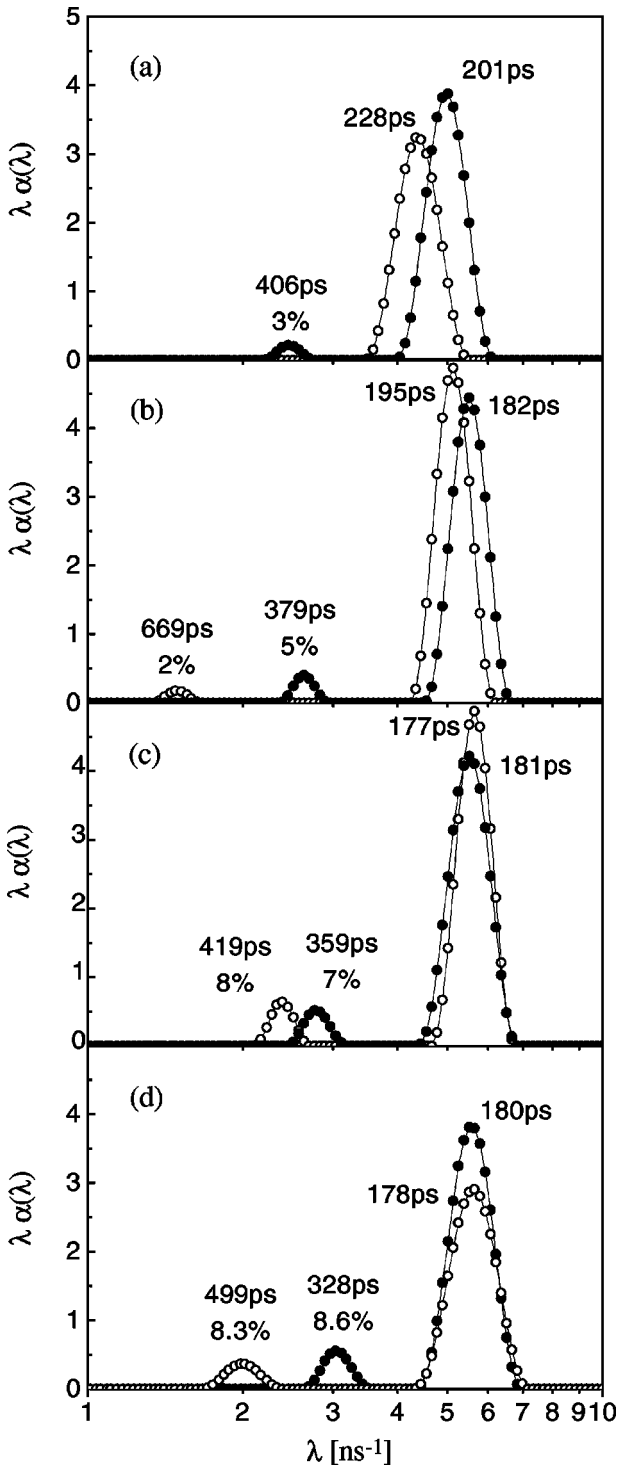

FIG. 2. Comparison of the positron annihilation rate distributions $f(\lambda)$ measured at 300 K (open circles) and 20 K (full circles) for four stages of thermal treatment: (a) as-quenched amorphous sample, (b) relaxed sample (573 K for 3 h), (c) sample after first crystallization (693 K for 1 h), and (d) sample after second crystallization (767 K for 1 h).

PDF is given by $f(\tau)=\lambda^2\alpha(\lambda)$. All results obtained from this analysis are shown in Figs. 2(a)–2(d) and in Table I. The results are determined with an accuracy of ± 3 ps and $\pm 1\%$ for the main lifetime and its intensity, respectively.

TABLE I. Positron lifetimes with the corresponding intensities I for four types of structure of Fe-Co-B obtained from $f(\lambda)$ measured at 300 and 20 K and recalculated to lifetime representation. Dashes indicate absence of the relevant lifetime in the PAL spectra.

Sample	τ_1 (ps)	I_1 (%)	τ_2 (ps)	I_2 (%)	τ_3 (ps)	I_3 (%)
			300 K			
amorphous	228	98			4085	2
relaxed	195	96	669	2	4987	2
1st cryst.	177	91	419	8	5435	1
2nd cryst.	178	90	499	8	4684	2
			20 K			
amorphous	201	97	406	3		
relaxed	182	95	379	5		
1st cryst.	181	93	359	7		
2nd cryst.	180	91	328	9		

III. RESULTS AND DISCUSSION

The Fe-Co-B sample in the amorphous state measured at room temperature exhibits a broad annihilation rate distribution $f(\lambda)$ with mean lifetime τ_1 of 228 ps. In all other cases and temperatures the results exhibit a second component τ_2 in addition to the unusually broad main annihilation component τ_1 with over 90% of the total intensity. A weak third component, τ_3, is present in all distributions at 300 K; this component likely reflects the intrinsic properties of the amorphous structure itself and cannot be assigned to the configuration of 12-layer stacked sample necessary for measurements. The third component τ_3 vanishes at low temperature and thus its origin remains unclear because it cannot be explained simply by thermal contraction of a complex void structure.

Positrons injected into a metallic glass fall into localized states[10] in regions of lower-than-average electron density. From Figs. 2(a)–2(d) it is seen that almost all positrons are trapped at sites with lifetimes τ_1 between 178 and 220 ps (Table I). These sites could not be attributed to bulk Fe or Co (or B) nor to vacancy defects [positron lifetimes in monocrystals are 110 ps for Fe (bcc) and 130 ps for Co (fcc),[11] in monovacancies 175 ps for Fe (bcc),[12,13] 167 ps for Co (hcp),[14] and 229 ps for pure boron powder[15]]. Because the amorphous metallic glasses are structurally disordered, the concept of vacancies (as in a perfect lattice) has no significance in these systems. Thus the information provided by PAL spectroscopy of amorphous metallic alloys essentially concerns the free volume V_f on an atomic-size scale or a vacancylike open volume (small subvacancy-sized free volume or excess free volume) inside the structure.

It is important to consider the contribution of the phonon scattering to the positron results, especially with respect to the measurements at low temperatures. The temperature dependence of the electrical resistivity in a wide temperature range from 4.2 K to hundreds of kelvins has allowed an analysis of the positron-phonon interactions in this kind of amorphous structure from the estimation of the phonon contribution to the overall electron scattering. The ratio of the ''phonon'' scattering contribution to the ''structure-

dependent'' or ''disorder'' contribution of the charge scattering mechanisms is small. The temperature dependence of resistivity shown in Fig. 1 indicates the dominance of the structure-dependent resistivity, which remains similar for different states of the amorphous matter, from the as-quenched state through both stages of crystallization until the completely recrystallized state is achieved. It can thus be inferred that the electron-phonon interaction is overridden by interaction of conduction electrons with structure units that persist until very high temperature. (The ratio of residual resistivity to the overall resistivity or to its temperature coefficient is unusually high for a metallic sample.) Thus we exclude the positron-phonon contribution to the value of the positron annihilation rate (trapping rate of positrons) as only weakly temperature dependent. Also, due to the highly ''defective'' (i.e., disordered) character of the metallic glassy sample, saturation of the positron trapping can be expected to be the main process controlling the positron annihilation rate in this material, the spectrum being almost completely dominated by the ''defect'' component τ_1.[16]

Comparison of $f(\lambda)$ at room and at low temperature for the amorphous as-quenched states, Fig. 2(a), shows a shift to higher values of λ (toward lower values of V_f) for lower temperatures; in addition, a second peak appears in the spectra. In positron lifetime representations this result means a decrease from 228 ps to 201 ps and the second peak at 406 ps appears with an intensity of 3%. In addition to the presence of inherent small free volumes due to atomic disorder, the amorphous state also contains excess free volume. Due to the disorder of the surrounding atomic structure a continuous free volume distribution $f(V)$ is to be expected. Two effects can be deduced from the positron annihilation rate distributions for the amorphous structure in the graph in Fig. 2(a). Thermal contraction is reflected in a ''lattice'' contraction of the amorphous structure leading to a decrease in τ_1 by about 28 ps. Furthermore, thermal contraction at low temperatures may lead to the concentration, rather than relaxation, of excess free volume dispersed in the entire sample volume into larger open spaces responsible for the generation of the second peak at 20 K. As metallic glasses are known to contain no dislocation lines, loops, or grain boundaries that might act as shallow traps, the appearance of the second annihilation peak in the spectrum at 20 K can hardly be explained by the process of thermal detrapping of positrons from such structures upon temperature increase. The second peak reappears unchanged after temperature cycling to 300 K and then to 20 K again, indicating no noticeable low-temperature (irreversible) relaxation behavior in this amorphous alloy. The main annihilation peaks are unusually broad at both temperatures.

After annealing the sample to relax the excess free volume at 573 K for 3 h, measurements performed on the still-amorphous sample exhibit a further shift of $f(\lambda)$ to a higher value of λ (lower value of V_f). The decrease of excess free volume in the as-quenched structure upon annealing has been invoked also by other workers to explain the observed changes during structural relaxation.[17] The lifetime τ_1 decreases to 195 ps (by about 33 ps, Table I), reflecting the increase in the density of the amorphous structure due to relaxation. The decrease of τ_1 with decreased measuring

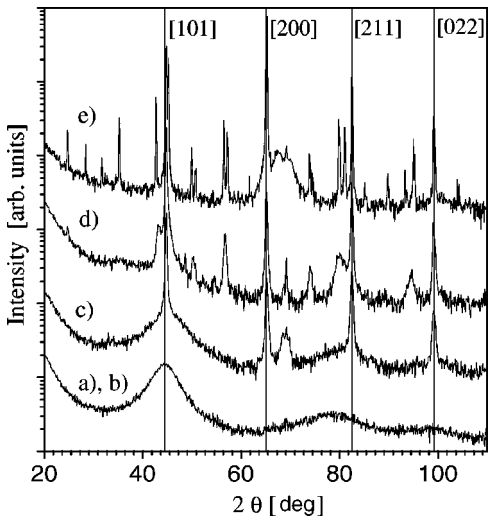

FIG. 3. X-ray patterns for all annealing stages, including high-temperature recrystallization: (a) amorphous as-quenched, (b) amorphous relaxed, (c) 693 K for 1 h (amorphous and α-FeCo), (d) 767 K for 1 h [α-FeCo+$(FeCo)_3B$], and (e) 1000 K for 1 h [α-FeCo+$(FeCo)_2B$]. Vertical lines are reflections of α-FeCo.

temperature is now only 13 ps [Fig. 2(b)], a value that is quite reasonably attributed to thermal contraction of the capture sites, the structure being now well relaxed yet fully amorphous. A thermal contraction of the entire relaxed structure will shorten interatomic distances in the constituent structure units and redistribute the remaining free volume. This contraction and redistribution of free volume may justify the appearance of the second distribution in $f(\lambda)$ (redistribution of free volume to larger regions during the thermal relaxation of the amorphous structure), which contracts with decreasing temperature: τ_2 decreases from 669 to 379 ps, but doubles in intensity. Note that all changes take place in the relaxed disordered but still amorphous state, as checked thoroughly by both x rays and TEM.

After the first crystallization reaction [Fig. 2(c)], the $f(\lambda)$ shifts further toward higher λ (τ_1 decreases from the previous 195 to 177 ps) and the annihilation rate distributions remain essentially the same at 20 K also. The second lifetime peak τ_2 falls from the value of 669 ps in the relaxed state to 419 ps after the first crystallization reaction and with decrease of temperature down to 359 ps. The intensity of the second lifetime peak increases from 2% in the relaxed state to 8% and with decreasing temperature slightly decreases to 7%. It is known from previous work that during the first crystallization reaction α-FeCo crystals with grain sizes of about 100 nm are produced from the amorphous metallic matrix, as shown by TEM,[7] and with x-ray diffraction (Fig. 3), leaving metal-metalloid clusters embedded in the amorphous state. These clustered amorphous regions transform during the second crystallization into $(FeCo)_3B$ borides and additional α-FeCo. The micromechanism of the formation of the first crystalline phase from the amorphous state with respect to the atomic structure of the amorphous state is analyzed in great detail in Refs. 7 and 17 in binary Fe-B and ternary Fe-Co-B systems, and the results will be useful for interpretation of the uncommonly weak temperature depen-

dence of the first positron annihilation peaks in Fig. 2(c).

After the second crystallization at 767 K [Fig. 2(d)], the sample again gives a positron annihilation rate distribution with one main peak of $f(\lambda)$ and produces also a second peak with an intensity of 8%. The value of τ_1 is 50 ps lower than τ_1 in the amorphous state; $f(\lambda)$ is again unaffected by the temperature decrease and is the same as it was at 300 K within the limit of accuracy. The lifetime τ_2 increases from 419 to 499 ps with increasing crystallization and decreases with decreasing temperature to 328 ps. The intensities of the second peak remain practically the same.

Comparing Figs. 2(c) and 2(d), it can be seen that the formation of new boride phases does not change the main peak of the positron annihilation rate PDF $f(\lambda)$, although almost 50% of the sample volume (amorphous remains left over after the first crystallization reaction) has transformed to crystalline phases. Thus it seems that the main positron trapping occurs on structures that are not directly related to the specific crystalline phase, or to the boundaries between crystalline and amorphous phases appearing after the first crystallization reaction, or to the interfaces between crystalline grains after the second crystallization reaction.

The specific behavior of the main annihilation rate peak with devitrification and temperature change and the unusually broad shapes of the main peaks suggest the presence of at least two rather similar positron capture sites within the atomic arrangement of the rapidly quenched Fe-Co-B amorphous structure throughout the whole devitrification process. Over 92% of all positrons annihilate in these sites, yielding one main broad annihilation peak well separated from the second minor ($<8\%$ in intensity) peak.

Two kinds of capture sites

To verify the assumption about the existence of two types of positron capture sites we have decomposed the main annihilation rate distribution into two distributions. This procedure was made possible by refining the CONTIN Laplace inversion procedure to compute a fine-scale distribution function $f(\lambda)$. Prior to this decomposition we checked the stability of the solutions obtained, e.g., for different deconvolution intervals, different numbers of grid points, and different numbers of constituent components. The results of decomposition of the main component of the annihilation rate PDF's, $f(\lambda)$, but in positron annihilation lifetime representation PDF's, $f(\tau)$, into two components with corresponding lifetimes τ_{11} and τ_{12} are summarized in Table II.

To interpret these results we have made use of a structure model of SRO of iron and boron atoms according to Ref. 18, where it is shown that boron in the ''amorphous'' structure is surrounded by six iron atoms and forms a so-called bridging complex, which should be stable and exist until the last crystallization stage. The schematic amorphous Fe-Co-B structure, approximated for convenience by bcc unit cells (these being the first crystalline phases formed during crystallization of this alloy) with the described local ordering is exhibited in Fig. 4, adapted for our case from the crystallographic scheme for binary ''amorphous'' Fe-B.[18] In such a locally ordered structure there are two possible sites for positron capture. These two sites have identical atomic surroundings but differ in the surrounding electron density due to the presence of different kinds of interatomic bonding. The first site with positron lifetime denoted as τ_{11} is located in the intermediate space between the complexes; it is surrounded by metal bonds and its size and occurrence should be affected more strongly by the presence of additional metal atoms. The second site with positron lifetime denoted as τ_{12} is located close to the center of the complex, and in the proximity of the metal-metalloid bonds in the bridging complex, where the surrounding electron density is reduced due to the strength and metal-metalloid (semicovalent) character of the (FeCo)-B bonds inside the bridging complex. The site τ_{12} should remain unaffected by crystallization from the amorphous state, because the complexes are structurally similar to the arrangement in the Fe_3B borides.

TABLE II. Decomposition of the main peak of $f(\lambda)$ into two components recalculated to lifetime representation, τ_{11} and τ_{12}.

Sample	τ_1 (ps)	I_1 (%)	τ_{11} (ps)	I_{11} (%)	τ_{12} (ps)	I_{12} (%)
			300 K			
amorphous	228	98	222	70	245	28
relaxed	195	96	191	71	208	25
1st cryst.	177	91	173	66	189	25
2nd cryst.	178	90	173	65	193	25
			20 K			
amorphous	201	97	196	71	216	26
relaxed	182	95	177	67	193	28
1st cryst.	181	93	176	66	195	27
2nd cryst.	180	91	175	65	194	26

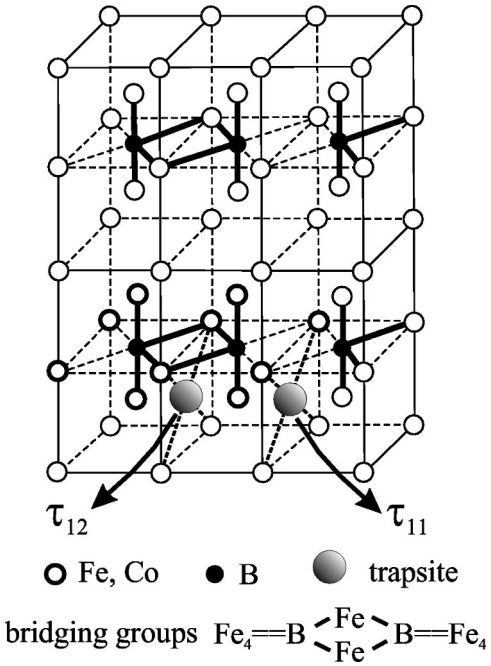

FIG. 4. Structural model of SRO of Fe/Co and B atoms in amorphous structure showing bridging complexes and two possible positron capture sites.

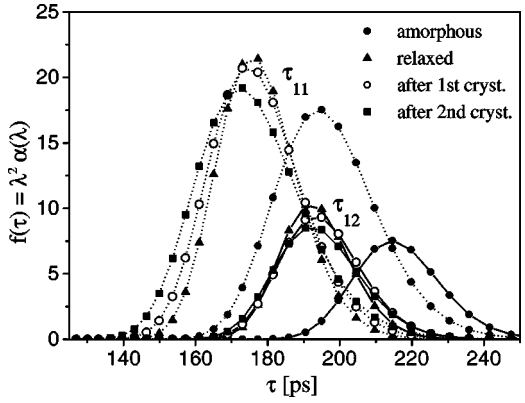

FIG. 5. Annihilation lifetime PDF's $f(\tau)$ obtained by decomposition of the main peaks of $f(\lambda)$ into two components, which represent two kinds of capture sites, for four types of structure, namely, amorphous as-quenched sample, amorphous relaxed sample, sample after the first crystallization stage, and fully crystalline sample after the second crystallization, measured at low temperature (20 K).

The preference of a delocalized positron for different components in a given heterostructure (or host matrix and clusters) is given by the positron affinity *A*, a negative number that is the sum of electron and positron chemical potentials. A larger negative value means that the positron has a stronger preference for the material in question. It is to be noted that the differences in positron affinities *A* of the relevant metal atoms are small, e.g., of the order of 0.3 eV [$A(\mathrm{Fe}) = -3.83$ eV, $A(\mathrm{Co}) = -4.18$ eV (Ref. 19)]. For this reason no significant influence of positron affinity of these atoms on the lifetime of the positrons is expected.

The data in Table II show that at 300 K the value of the first lifetime τ_{11} decreases from 222 ps in the amorphous state, relaxing through 191 ps, and decreasing to 173 ps upon crystallization. Similar behavior of τ_{11} is observed at low temperature. The intensities I_{11} of this annihilation peak after relaxation attain 65% at both temperatures. This decrease is monotonic at both temperatures. The behavior of τ_{11} at different annealing stages indicates the evolution of the sites that are close to metal-rich regions (τ_{11}). Graphically the evolution of annihilation at this site in the lifetime representation $f(\tau)$ is presented in Fig. 5 (dotted lines, annihilation lifetime PDF in sites between bridging complexes at 20 K), where the tendency to shift toward shorter lifetimes observed in polycrystalline systems[20] with annealing is visible and may be expected to be attained after very-high-temperature annealing (above 1000 K).

The behavior of τ_{12} at room temperature indicates that in the early stages of nucleation the positron annihilation lifetime at this site already attains a value close to the final value of 193 ps observed after the second crystallization stage. This value of τ_{12} and an almost identical intensity are attained at low temperatures after relaxation of excess free volume. The intensity I_{12} of this annihilation peak exhibits a nearly constant value, which reflects the number of previously described positron traps at sites with reduced electron density. Figure 5 (full lines) shows that the distribution $f(\lambda)$ (in the lifetime representation) at the sites that are supposed to correspond to centers of the bridging complexes is positionally fixed. This result reflects the stability of the SRO in the bridging complexes against all induced structural changes. A slight decrease in the intensity of this annihilation peak indicates a small decrease in the number of bridging complexes during the transformation process.

The overall behavior of $f(\tau)$ for both sites, shown in Fig. 5, indicates high stability of the two sites (τ_{11} and τ_{12}) against crystallization from the amorphous structure. The two kinds of sites, which represent two different kinds of traps for positrons and the stability of the SRO in the bridging complexes in the vicinity of which the trap are localized explain well the observations in Figs. 2(c) and 2(d), where the overall (undecomposed) main peak of $f(\lambda)$ is shown to reflect only very weakly the influence of the two crystallization stages and of measuring temperature. This observation is explained by the assumption that only one of the sites (τ_{11}) is affected by these processes. Even high-temperature annealing at 767 K does not seem to lead to a complete disappearance of the SRO present in the bridging complexes, although complete devitrification has already taken place, as can be seen from the x-ray diffraction pattern [curve (d) in Fig. 3]; loss of this SRO may be expected after recrystallization at 1000 K [curve (e) in Fig. 3], where a complete atomic rearrangement takes place, but in the crystalline state. The presence of such stable ordered microstructures also supports the idea that all structure rearrangements upon transition from the amorphous to the crystalline state are controlled by cooperative motion and slight rearrangement of entire complexes.

The existence of such bridging complexes in the amorphous (relaxed) structure leads to a question about their origin. Since the high quenching rates achieved during sample preparation make the idea of complex formation during cooling improbable, the high thermal stability of these complexes and measurements of magnetic properties of similar melts[21] suggest that this SRO is present already in the melt and is preserved by rapid quenching.

IV. CONCLUSIONS

Amorphous alloys represent a highly disordered structure, yet with well-defined short-range order. Two types of trapping sites for the annihilation of positrons can be identified in Fe-Co-B metallic glasses. These sites reflect the short-range atomic ordering present in the amorphous structure. The location of one trapping site is close to the center of metal-metalloid coordination and reflects the bridging complex; the other trap is located in intermediate spaces between complexes that are surrounded mostly by metal atoms. The original quenched-in SRO persists until full crystallization. Different ratios of the number of traps of each type can be expected in samples with different degrees of clustering of Fe or Co around B atoms.

ACKNOWLEDGMENTS

The authors express their thanks to the Grant Agency for Science of Slovakia for the support of this research (Grant No. 2/6064/99).

[1] J.D. Bernal, Proc. R. Soc. London, Ser. A **280**, 299 (1964).
[2] G. S. Cargill III, *Atomic Energy Review*, Suppl. No. 1 (IAEA, Vienna, 1981), p. 63; G.S. Cargill III, Solid State Phys. **30**, 227 (1975).
[3] K. Sugiyama, A. Shinohara, Y. Waseda, and A. Inoue, J. Non-Cryst. Solids **193**, 376 (1995).
[4] K. Krištiaková, P. Švec, J. Krištiak, P. Duhaj, and O. Šauša, Mater. Sci. Eng., A **226-228**, 321 (1997).
[5] K. Krištiaková, P. Švec, J. Krištiak, O. Šauša, and P. Duhaj, J. Non-Cryst. Solids **192**, 277 (1995); K. Krištiaková, J. Krištiak, P. Švec, O. Šauša, and P. Duhaj, Mater. Sci. Eng., B **39**, 15 (1996).
[6] L. Kraus, V. Hašlar, P. Duhaj, P. Švec, and V. Studnička, Mater. Sci. Eng., A **226-228**, 626 (1997).
[7] P. Duhaj and P. Švec, Key Eng. Mater. **40&41**, 69 (1990).
[8] V.Z. Bengus, E.D. Tabachnikova, P. Duhaj, and V. Ocelík, Mater. Sci. Eng., A **226-228**, 823 (1997).
[9] R.B. Gregory and Y. Zhu, Nucl. Instrum. Methods Phys. Res. A **290**, 172 (1990).
[10] R.P. Gupta, Solid State Commun. **65**, 93 (1988).
[11] A.G. Balogh, L. Bottyan, G. Brauer, I. Dézsi, and B. Molnár, J. Phys. F: Met. Phys. **16**, 1725 (1986).
[12] A. Vehanen, P. Hautojärvi, J. Johansson, J. Yli-Kauppila, and P. Moser, Phys. Rev. B **25**, 762 (1982).
[13] A. Seeger, F. Banhart, and W. Brauer, in *Positron Annihilation*, edited by L. Dorikens-Vanpraet, M. Dorikens, and D. Seeger (World Scientific, Singapore, 1989), p. 275.
[14] S. Dannefaer, D.P. Kerr, S. Kupca, B.G. Hogg, J.U. Madsen, and R.M.J. Cotterill, Can. J. Phys. **58**, 270 (1980).
[15] Khalid Al Ani, I. Dézsi, Zs. Kajcsos, A. Balogh, B. Molnar, and G. Brauer, KFKI Report No. 1981-03, Central Research Institute for Physics (unpublished).
[16] M.J. Puska and R.M. Nieminen, Rev. Mod. Phys. **66**, 841 (1994).
[17] R. Dittmar, R. Würschum, W. Ulfert, H. Kronmüller, and H.-E. Schaefer, Solid State Commun. **105**, 221 (1998); C. Nagel, K. Rätzke, E. Schmidtke, J. Wolff, U. Geyer, and F. Faupel, Phys. Rev. B **57**, 10 224 (1998).
[18] P. Duhaj and F. Hanic, Phys. Status Solidi A **76**, 476 (1983).
[19] M.J. Puska, P. Lanki, and R.M. Nieminen, J. Phys.: Condens. Matter **1**, 6081 (1989).
[20] W. Trifthäuser and G. Kögel, in *Metallic Glasses: Science and Technology*, edited by C. Hargitai, I. Bakonyi, and T. Kemeny (Kultura, Budapest, 1981), p. 347.
[21] W. Weiss and H. Alexander, J. Phys. F: Met. Phys. **17**, 1987 (1983).